

PAPER

Small non-uniform basal crystal fields in HVPE free-standing GaN:Mg as evidenced by angular dependent and frequency-dependent EPR

To cite this article: U R Sunay *et al* 2019 *J. Phys.: Condens. Matter* **31** 345702

View the [article online](#) for updates and enhancements.



IOP | ebooks™

Bringing you innovative digital publishing with leading voices to create your essential collection of books in STEM research.

Start exploring the collection - download the first chapter of every title for free.

Small non-uniform basal crystal fields in HVPE free-standing GaN:Mg as evidenced by angular dependent and frequency-dependent EPR

U R Sunay¹, M E Zvanut^{1,4}, J Marbey², S Hill², J H Leach³ and K Udway³

¹ Department of Physics, University of Alabama at Birmingham, Birmingham, AL 35294, United States of America

² Department of Physics and NHMFL, Florida State University, Tallahassee, FL 32310, United States of America

³ Kyma Technologies, Inc., Raleigh, NC 27617, United States of America

E-mail: mezvanut@uab.edu

Received 7 March 2019, revised 1 May 2019

Accepted for publication 16 May 2019

Published 6 June 2019



Abstract

We studied thin-film and free-standing Mg-doped GaN using multi-frequency electron paramagnetic resonance (EPR) at 3–3.5 K and 9.4–130 GHz. Free-standing samples exhibit a highly anisotropic intensity, varying by a factor of 20 from 0° to 60°. In contrast, the intensity of the thin-film samples is significantly more isotropic, varying by no more than 10% over the same range of angles. The angular dependent intensity can be modeled in both free-standing and thin-film samples similarly to the g -factor anisotropy reported for thin films, supporting the theoretical predictions that the hole is on a basal site around the Mg acceptor. In addition, frequency-dependent transmission EPR measurements reveal a distribution of g_{\perp} in free-standing samples, indicating that the local basal crystal field is non-uniform.

Keywords: GaN, Mg, multifrequency EPR, freestanding, shallow acceptor, strain

(Some figures may appear in colour only in the online journal)

Introduction

Gallium nitride (GaN) is a semiconductor with a direct bandgap of 3.44 eV that can be altered by alloying with In or Al to achieve the most well-known application, a light emitting diode [1, 2]. Additionally, the high breakdown voltage, saturation velocity, and electron mobility make it an excellent material for high-power high-frequency electronic devices [3, 4]. For many of the high-power applications to be achieved, homoepitaxial growth is preferred due to the myriad of issues from defects caused by heteroepitaxial growth, such as reduced thermal conductivity, reduced device performance and lifetime, and increased biaxial strain [5–8].

The successful technological applications are only possible because GaN can be doped as both n-type and p-type. The

former is achieved by minimizing the free carriers inherent to most growth conditions and controlled introduction of Si. The latter proved more challenging, but now is routinely realized by doping GaN films with Mg. Despite the importance attributed to the Mg dopant, most of the fundamental structural information about the acceptor is provided by theory. To assist in visualization of the Mg defect in GaN, a schematic of Mg_{Ga} and the neighboring atoms in wurtzite GaN is shown in figure 1. All results indicate that Mg substitutes for Ga and the hole resides mostly on the near neighbor nitrogen atom. But density functional theory (DFT) calculations are currently unable to determine whether the hole prefers the axial or one of three basal nitrogen sites shown in figure 1 because the energy levels of the electronic ground state are within the uncertainty of the calculation [9, 10]. Typically, the detailed structure of an impurity may be experimentally probed by magnetic resonance studies that can determine the unpaired

⁴ Author to whom any correspondence should be addressed.

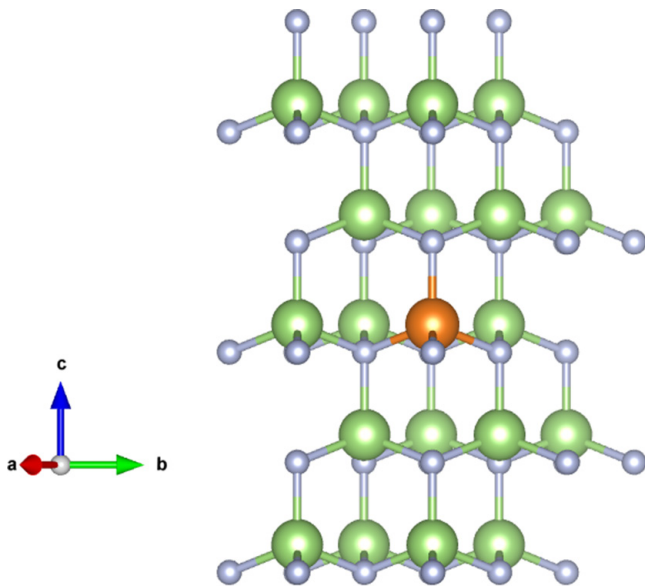


Figure 1. Schematic of Mg (orange sphere) substituting at a Ga (green) site surrounded by 4N (silver) atoms in hexagonal GaN. **a**, **b**, and **c** are the hexagonal crystal axes. The basal plane, mentioned in the text, is the crystal *ab* plane. The axial nitrogen is a nearest neighbor to Mg lying along the *c*-axis; the basal nitrogen are nearest neighbors in the basal plane.

spin distribution through examination of the electron-nuclear hyperfine interaction. Not surprisingly, such information is unavailable for Mg in GaN, likely due to spectral broadening caused by the 100% abundant nuclear spins of Ga and N and sample strain. To date, the only spectroscopic information about Mg is the *g*-factor, a parameter derived from the interaction of the paramagnetic electron with the surrounding crystal. Nevertheless, a magnetic resonance study of heteroepitaxial films, combined with secondary ion mass spectroscopy (SIMS) and photoluminescence (PL), convincingly associated an isotropic 100 G peak-to-peak broad resonance at 9.4 GHz near $g = 2$ with the Mg acceptor [11]. Later, Glaser *et al* attributed a highly anisotropic signal seen in homoepitaxial films to the same Mg acceptor and accounted for the different spectral characteristics by the relief of non-uniform strain inherent to heteroepitaxial films [12]. Armed with only the electron paramagnetic resonance (EPR) *g*-factor, Aliev *et al* applied crystal field theory to the hole at the Mg acceptor in GaN, and demonstrated that signals seen in the heteroepitaxial and homoepitaxial films could be adequately described by a hole residing on a basal nitrogen subject to a non-axial crystal field [13]. Malyshev arrived at a similar conclusion employing localized valence band wave functions rather than the simple p-orbital used in the work of Aliev [14]. Both models, then, suggest that the hole is basal, rather than axial. Alternatively, the angular dependent EPR data could also be accounted for by a model developed by Alves *et al* in which the Mg hole is delocalized over all four neighboring N atoms [15].

The interpretation of magnetic resonance data is further complicated by an angular-dependent spectral broadening that varies from sample to sample. The broadening is particularly evident in the EPR studies of free-standing crystals reported in [13]. The observations were attributed to non-uniform

strain that was minimized in the thick free-standing crystals and maximized in thin heteroepitaxial films. Significantly, evidence for non-uniform strain in the EPR spectra implies that such strain directly affects the Mg acceptor.

The model of the Mg acceptor derived from experiment thus far states that the hole prefers a basal nitrogen and is subject to the non-uniform strain created by the crystal growth conditions. However, the model is based solely on one parameter, the EPR *g*-factor. Another feature of the EPR that can be analyzed is the intensity. A comparison of the EPR intensity with that predicted by the crystal field model was limited in the past by the small variation observed in the spectral intensity of heteroepitaxial films and low signal-to-noise ratio observed for homoepitaxial films. However, the significantly improved signal-to-noise ratio and highly anisotropic spectral intensity provided by thick free-standing Mg-doped crystals provides an opportunity to test the crystal field model and the important conclusion regarding the localization of the hole. In addition, the strain non-uniformity predicted in earlier work may be investigated by frequency-dependent measurements since non-uniformity implies that the linewidth depends on the microwave frequency used to detect the signal. Given the importance of the Mg-acceptor in GaN technology, we tested the crystal field model of Aliev *et al* by examining the angular dependent intensity in both heteroepitaxial thin-films and free-standing crystals. Furthermore, the suggested non-uniformity was investigated by measuring the EPR signal over a range of frequencies between 50 to 130 GHz. All results confirm that, in the ground state, the hole must reside on a basal nitrogen atom subjected to various strains, likely attributed to their location in the crystal.

Experimental parameters

GaN:Mg films were grown on sapphire substrates by metal modulated epitaxy (MME) and metal-organic vapor phase epitaxy (MOVPE) to a thickness of 0.3 μm and 0.5 μm , respectively. A collection of 3 MME and 4 MOVPE samples were examined for this study, and a representative sample from each set was chosen for presentation here. The Mg concentration in the MME sample is $1.5 \times 10^{20} \text{ cm}^{-3}$ and that in the MOCVD film is $5 \times 10^{19} \text{ cm}^{-3}$ as measured by SIMS. A representative sample from a collection of millimeter-thick crystals grown on sapphire by hydride vapor phase epitaxy (HVPE) was also studied. As the HVPE sample cooled after growth, the GaN separated from the substrate due to thermal stress and was polished, resulting in free-standing GaN doped with $3.0 \times 10^{18} \text{ cm}^{-3}$ Mg. The detailed growth process and additional characterization was described previously [16–19].

The intensity of a paramagnetic center is expected to be inversely proportional to the temperature of the system—the Mg^0 acceptor is no different. To improve the precision of our analysis, we go to the lowest achievable temperatures for the best signal to noise ratio. Angular-dependent EPR measurements were performed at 3.5 K using an X-band Bruker EPR spectrometer with the static magnetic field in a plane containing the *c*-axis and the microwave magnetic field perpendicular to

the static magnetic field. The angular-dependent zero-crossing of the Mg-related EPR signal was fit to a model with axial symmetry along the c -axis. The g -factors are determined from the standard resonance condition:

$$hf = \mu_B \vec{B}^T \cdot \vec{g} \cdot \vec{S} \quad (1)$$

where h is the Planck constant, f is the microwave frequency, μ_B is the Bohr magneton, and \vec{g} is the g -factor matrix for the defect. The corresponding g -factor matrix anisotropy for Mg in GaN can be expressed with two unique parameters given by the equation

$$g^2 = g_{\parallel}^2 \cos^2(\theta - \theta_0) + g_{\perp}^2 \sin^2(\theta - \theta_0) \quad (2)$$

where θ is the angle between the c -axis and the static magnetic field, g_{\parallel} and g_{\perp} are the g -factors with the static field parallel and perpendicular to the c -axis, respectively, and θ_0 accounts for initial sample misalignment. The intensity of the EPR signal was determined by numerical integration, including baseline subtraction. The relative uncertainty is estimated to be 10%.

EPR frequency dependent measurements were performed at 3.0 K in the range of 37–130 GHz. Microwave frequencies were generated using an ABmm Millimeter-wave Vector Network Analyzer in conjunction with a series of Schottky diodes to achieve harmonic multiplication as described by Mola *et al* [20]. The experiment was carried out in a transmission set up to avoid any distortion of the spectral line shape that would otherwise be present in a typical cavity perturbation measurement where the sample exhibits strong dispersion. Phase-amplitude mixing was minimal, but nevertheless corrected for in post processing data analysis. Transmission line-shapes were fit to a Lorentzian function and the full width at half maximum is reported. Frequency-dependent linewidth results equivalent to those reported in this paper have also been observed in absorption cavity EPR systems in other HVPE Mg-doped free-standing samples.

The angle-dependence of the g -factor and spectral intensity are determined by the axial crystals field Δ_z , non-axial field Δ_x , spin-orbit coupling λ , and orbital g -factor g_1 , as was noted in earlier work [13, 21]. In the present work, we optimize Δ_x to best fit the calculated and experimental angular intensity dependent data and report the subsequent g -factor anisotropy. To calculate EPR intensities and g -factors, wavefunctions were calculated using $2p$ orbitals and applying the Hamiltonian used by previous authors that successfully explained the Mg g -anisotropy [13]

$$H = \Delta_z [\hat{L}_z^2 - l(l+1)/3] + \Delta_x [\hat{L}_x^2 - l(l+1)/3] + \lambda \mathbf{L} \cdot \mathbf{S}. \quad (3)$$

A Hamiltonian including both x and y orbital operators reflecting strain directed along the basal bonds had little effect on the agreement between calculations and experimental results.

EPR g -factors were computed by using

$$g_x = 2 \left| \left\langle i \left| \left(g_e \hat{S}_x + g_1 \hat{L}_x \right) \right| j \right\rangle \right| \quad (4a)$$

$$g_y = 2 \left| \left\langle i \left| \left(g_e \hat{S}_y + g_1 \hat{L}_y \right) \right| j \right\rangle \right| \quad (4b)$$

$$g_z = 2 \left| \left\langle i \left| \left(g_e \hat{S}_z + g_1 \hat{L}_z \right) \right| i \right\rangle \right| \quad (4c)$$

where g_e is the free electron g -factor factor of 2.002319, g_1 is the orbital reduction factor, and $|i\rangle$ and $|j\rangle$ are the degenerate ground state wavefunctions obtained from equation (3)[22]. To maintain axial symmetry, $g_x \approx g_y = g_{\perp}$, the axial crystal field was constrained such that $|\Delta_z| \gg |\lambda|$ and $|\Delta_z| \gg |\Delta_x|$. Additionally, the sign of the axial crystal field was negative and $g_1 = 0.10$ so that calculated g -factors could match the experimental anisotropy, as explained by previous authors. In the spin-orbit coupling term, λ was chosen to be -1 meV, in agreement with the factor found in homoepitaxial GaN [23]. The axial field values in the first term were -5 meV and -15 meV for the free-standing and thin-film calculations, respectively. These axial crystal field values are similar to those found from photoreflectance spectroscopy reports in GaN thin-films [24]. A potential explanation for the small orbital reduction factor g_1 and spin-orbit coupling term λ is electron-phonon coupling in the form of a dynamic Jahn-Teller effect, as suggested in previous papers [14, 25].

The EPR intensity was calculated by

$$I \propto |\langle i' | H_{mw} | j' \rangle|^2 \left(\frac{d(E_i - E_j)}{dB} \right)^{-1}, \quad (5)$$

where the first term is the transition matrix element due to the perturbing microwave field and the second term is the frequency-to-field conversion factor which is proportional to $1/g$ [26, 27]. The dipole moment operator associated with the microwaves incident on the sample is $H_{mw} = \mu_B B_1 g_{\perp} \hat{S}_{\perp}$, where B_1 is the amplitude of the microwave magnetic field. In thin-film samples, the intensity is almost entirely dependent on the second term of equation (5), i.e. proportional to $1/g$, and the transition matrix element is nearly isotropic. Conversely, for the free-standing samples, the intensity depends more strongly on the transition matrix overlap than it does the g -factor; therefore, first order corrections to the ground states $|i\rangle$ and $|j\rangle$ used previously were calculated and are reported here as $|i'\rangle$ and $|j'\rangle$. Second and third order correction terms were inspected but were too small to affect the results.

Results and discussion

The angular dependence of the g -factor in the thin films and free-standing sample are similar to those reported by others. In figure 2, the former is represented by filled squares and the latter by unfilled circles, and the solid lines are fits using equation (2). For the free-standing sample, $g_{\parallel} = 2.18$ and $g_{\perp} = 0.28$, but note that the value of g_{\perp} depends critically on spectra obtained at angles approaching 90° which occur at magnetic fields beyond the range of the 1 T magnet. Thin-film MOVPE g -factors were determined to be $g_{\parallel} = 2.08$ and $g_{\perp} = 1.99$ and those of the MME sample, $g_{\parallel} = 2.06$ and $g_{\perp} = 2.01$. The g -factor anisotropy is consistent with

earlier work [12, 19, 28]. As discussed by others, the g -factor anisotropy seen in the thin-film samples ($g_{||} - g_{\perp} = 0.09$ and $g_{||} - g_{\perp} = 0.05$) compared to the free-standing crystals ($g_{||} - g_{\perp} \approx 1.9$) reflects a decrease in the local non-axial crystal field Δ_x [13, 14]. The trend is continued qualitatively in the films, where the more heavily doped, thinner MME samples exhibit a smaller $g_{||} - g_{\perp}$ than the MOCVD samples.

The same crystal field model used to explain the g -anisotropy should also be able to predict the intensity of the EPR spectra. That is, in addition to the basal crystal field Δ_x playing a dominant role in g -anisotropy, it has been predicted that both axial and basal crystal fields can significantly change the angular dependent intensity. Here we provide experimental evidence of this claim. The filled squares in figure 3(a) illustrate the angular dependence of the intensity for the free-standing sample. We first consider a model using only an axial crystal field (i.e. $\Delta_x = 0$), a method previously used to model shallow acceptors [15, 21]. The calculated EPR intensity is plotted as the dotted blue line in figure 3(a) [21]. The predicted EPR intensity should be proportional to $\tan(\theta)$ only when $(g_{\perp}/g_{||}) \tan(\theta) \ll 1$ where g_{\perp} and $g_{||}$ are the experimentally determined g -factors obtained from equation (2). Thus, one would expect the calculation to agree with the data well at small angles and begin to deviate at the larger angles. In fact, the opposite is seen. However, with the addition of a small non-zero non-axial crystal field term expected for free-standing thick crystals ($\Delta_x = 10^{-5}$ meV) the calculated angular dependent intensity becomes non-zero at 0° and matches well with experimental data at $0-60^\circ$ and $120-180^\circ$. We note that although the optimal Δ_x is small, the value must be non-zero and positive to fit the low angle data for free-standing samples as seen by the solid black line shown in figure 3(a). We acknowledge, however, that the small size of Δ_x suggests different factors may control the non-zero intensity. For instance, the addition of N 2s orbitals to the pure p-orbitals used here might have enough of an effect at parallel orientation as to induce a detectable EPR intensity without significantly altering the dramatic effects seen at perpendicular orientation, which is the focus of the model.

After finding the crystal field parameter that optimally fits the free-standing anisotropic intensity, g -factors are then computed using equations (3) and (4). The resulting g -factor calculations agree with the experimentally determined $g_{||}$, but deviate significantly from g_{\perp} . To investigate the source of this discrepancy, the angular dependence of the g -factor calculated from the intensity was compared with that determined by fitting equation (2) to the experimentally measured $g(\theta)$. Figure 2 shows the results, where the g -factors obtained from fitting the anisotropic intensity are represented by the dotted red line and those obtained from equation (2) are shown as the solid blue line. The comparison indicates that a discrepancy occurs only at angles near 90° , where spectra are not able to be measured. The differences between the g_{\perp} calculated from equation (1) and extracted from the intensity are therefore within the uncertainty of the $g(\theta)$ measurement.

The angular dependence of the intensity seen in the thin-films is minimal compared to that seen in the free-standing

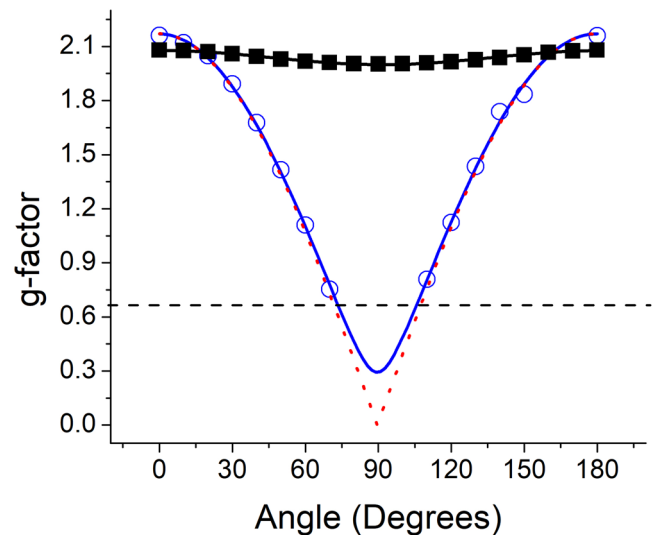


Figure 2. EPR g -factor angular dependence obtained at 9.4 GHz and 3.5 K by rotating the magnetic field in a plane containing the c -axis for thin-film MOVPE samples (black squares) and HVPE freestanding samples (blue circles). Lines are best fits to data using equation (1). Dotted red lines are g -factors extracted from fitting the intensity angular dependence. The horizontal dashed black line indicates the minimum g -factor accessible with the 1 T magnet at 9.4 GHz.

crystals and, therefore, limited information may be extracted. A comparison is shown in figure 3(b), where filled black squares represent the free-standing GaN and unfilled red circles the thin-films. The intensity of thin-film MOVPE samples varied less than 10% between 0° and 90° and could be simulated (red line) only with large axial and basal crystal fields. Consistent with the g anisotropy exhibited by the MOVPE and MME samples mentioned above, the intensity of the MME samples varied no more than 5% between 0° and 90° and the intensity calculations predict a larger crystal field. The smaller angle-dependent intensity, in addition to the decreased g -factor anisotropy, indicates that a larger crystal field exists in the MME samples compared to MOVPE. Using the same crystal field values as in the calculation of the angular dependent spectral intensity, a nearly isotropic g -factor was calculated and compared favorably with experimental results for both MOVPE and MME samples.

In the analysis of $g(\theta)$ performed by Aliev *et al*, a negative axial field was invoked to reproduce the observed relative values of $g_{||}$ and g_{\perp} ($g_{||} > g_{\perp}$). The negative Δ_z leads directly to the prediction that the hole resides on a basal, rather than axial, nitrogen. To verify the necessity of a negative axial field, intensity calculations were performed assuming a positive axial field or, equivalently, ground state axial hole. Although the results for the thin-films samples are non-conclusive due to the weak angular dependent intensity, the calculations for the free standing samples not only predict that $g_{\perp} > g_{||}$ as shown by previous authors, but that the EPR intensity decreases as the angle approaches 90° , consistent with the results shown in figure 3(a) [13, 15].

The source of the non-axial crystal field has, quite naturally, been attributed to physical strain because Δ_x is largest in the

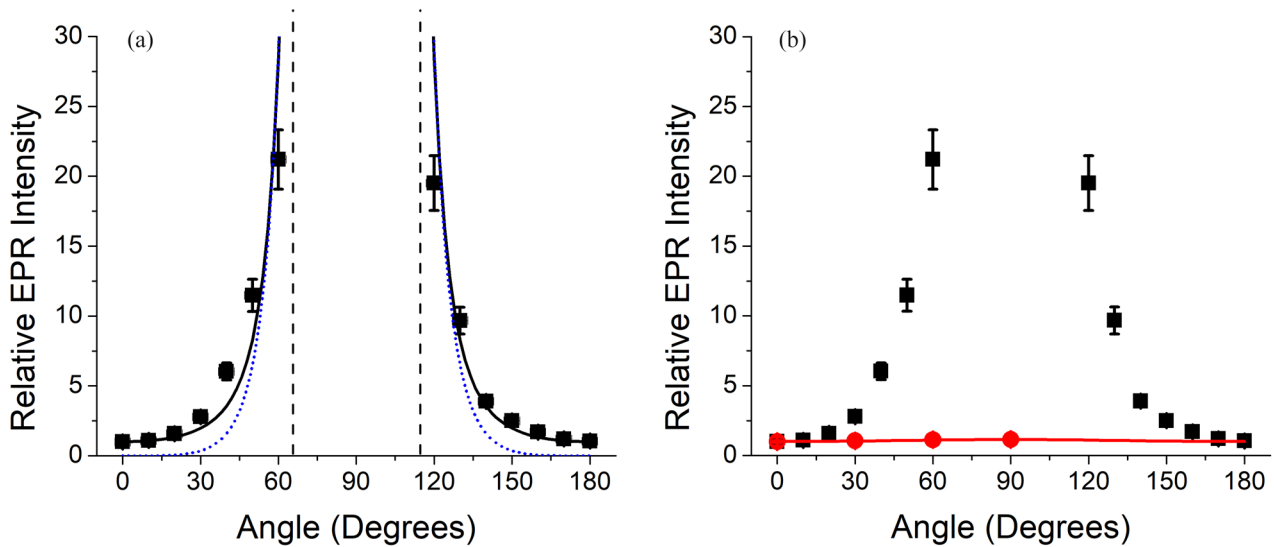


Figure 3. EPR Intensity angular dependence of (a) free-standing (black squares) and (b) both free-standing (black squares) and thin-film MOVPE (red circles) samples at 9.4 GHz. Solid lines are simulations of EPR intensity using the hamiltonian in equation (1). The dotted blue line in (a) is a fit using the same equation but with $\Delta_x = 0$. Vertical dashed black lines indicate inaccessible angles due to the signal's highly anisotropic g -factor.

thinnest films where dislocations and heteroepitaxially growth effects are the maximum [29]. However, random dislocations and interface mismatch need not be the sole contribution to the non-uniformity of the non-axial crystal field. For example, the 10^{18} cm^{-3} oxygen typical of ammonothermal GaN leads to a distance between randomly spaced O and Mg atoms of less than 10 nm, and should create large crystal fields in the vicinity of the Mg acceptor. Therefore, one would expect EPR characteristics similar to those seen in heteroepitaxially thin-films. Homoepitaxially grown ammonothermal p-type GaN doped with $8 \times 10^{18} \text{ cm}^{-3}$ Mg, were measured at 3.5 K and 10 GHz in the same manner as the samples discussed above. The results reveal a nearly isotropic EPR g -factor and intensity, consistent with the crystal field model.

Frequency dependence

In earlier work, a non-uniformity of the crystal field was deduced from an analysis of the angular dependent line shape. The study assumed that a non-zero distribution of g -factors (Δg), known as g -strain, caused the angular dependent line shape [12, 19, 30]. Each different g -factor, expressed as g_i , within the distribution of g -factors shifts the magnetic field resonance. Typically, the resonances due to each g_i in g -strained systems are not resolved, and produce instead a linewidth that increases with frequency.

To test for non-zero g -strain in these samples, EPR spectroscopy beyond the standard X-band system was required. Microwave frequencies from 50–130 GHz were obtained from a single Network Analyzer as described earlier and a 7 T magnet was required to record the complete EPR spectrum at angles closest to 90° . Figure 4(a) shows EPR transmission spectra of the Mg-related signal with the c -axis oriented at 5° and 40° from the static magnetic field \mathbf{B} at selected frequencies for free-standing GaN:Mg. The spectra shift horizontally,

as expected, due to the frequency dependence of the resonance evident in equation (1). The increase of the linewidth with frequency seen by a comparison of the spectra measured at about 50 GHz (lower) with those measured around 100 GHz (upper) provides evidence of g strain. Furthermore, the increase in linewidth at 40° compared to that at 5° reflects the greater sensitivity to non-axial strain expected for Δg_\perp compared with Δg_\parallel [13].

Samples with small non-uniform basal-crystal fields result in a non-zero Δg_\perp and a small Δg_\parallel as seen in previous crystal-field models [13, 14]. According to equation (2), at angles close to 0° , Δg_\parallel will be weighted heavily in determining linewidth broadening while Δg_\perp will have very little influence. The contribution from Δg_\perp increases, and from Δg_\parallel decreases, as the angle increases towards 90° . Since a small Δg_\parallel is predicted from the crystal field model for small non-uniform basal crystal fields, the linewidth should be relatively frequency independent at low angles. But as the angle increases, Δg_\perp , which is expected to be more sensitive to non-uniform basal fields, will contribute more to the linewidth and the EPR signal will broaden with frequency. This trend is shown by the frequency dependence of the linewidth in figure 4(b). At 5° the linewidth is almost frequency independent, reflecting the influence of a very small Δg_\parallel . On the other hand, the line width varies linearly with frequency as the angle between the c axis and applied magnetic field increases, indicating increasing contributions from Δg_\perp . The frequency dependence of the linewidth shown in figure 4(b) as well as the variation exhibited at different angles verifies the assumption of g -strain suggested by Zvanut *et al*, and provides further verification of the crystal field model suggested by Aliev *et al* [12, 19].

Included in the frequency-dependent data of figure 4(b) are three isolated points at 10 GHz. These data were obtained from the same samples measured at higher frequencies, but were measured in derivative mode using a conventional

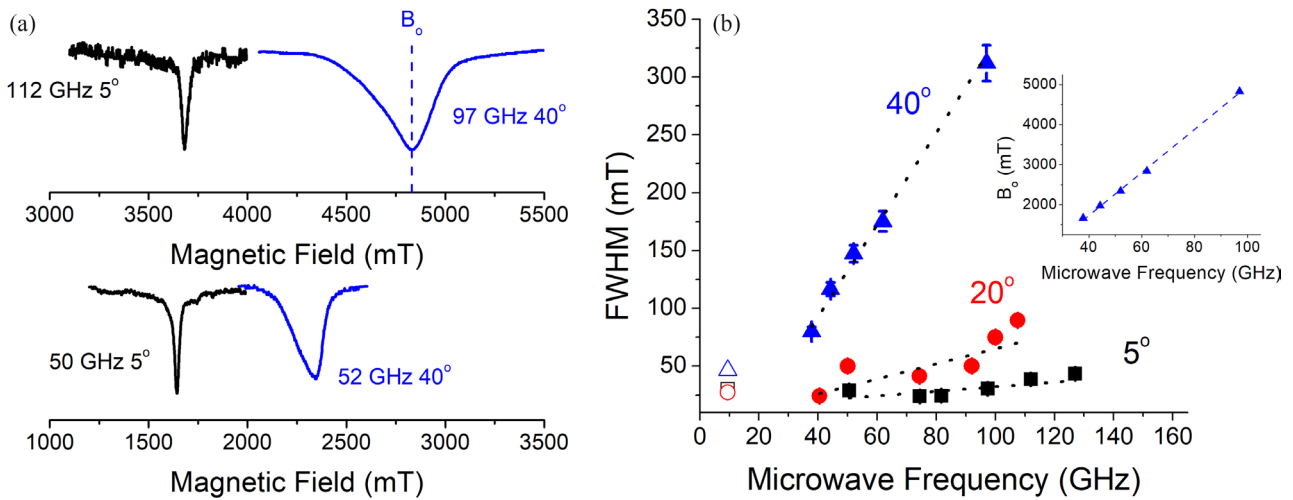


Figure 4. (a) EPR transmission spectra at 5° and 40° at two microwave frequencies and (b) frequency dependence of the FWHM of EPR spectra obtained from free-standing GaN:Mg measured with the angle between the c -axis and \mathbf{B} : 5° (black squares), 20° (red circles), and 40° (blue triangles). Dashed lines are linear fits. Unfilled symbols are the X-band results, where the symbols follow the same legend as higher frequency data. The inset shows the peak magnetic field at resonance B_0 as a function of microwave frequencies at 40° .

X-band spectrometer. Extrapolating from the data taken at higher frequencies suggests that the linewidth will not go through zero at 0 GHz, and that broadening mechanisms other than g -strain dominate at lower microwave frequencies. We suggest that a potential source of broadening is unresolved hyperfine splitting from neighboring Ga and N atoms. The delocalization of the hole wavefunction and the interaction strength with neighboring $I = 1$ nitrogen atoms and $I = 3/2$ Ga, each occurring with nearly 100% abundance, could ultimately determine the linewidth as the frequency is decreased, perhaps dominating at 10 GHz. Another potential frequency-dependent mechanism, crystal curvature, was dismissed due to the small size. For instance, x-ray diffraction measurements made across a 14 mm length, determined that the radius of curvature is 1.7 m for the free-standing samples and nearly 12 m for the thin-films. Neither contribute more than 3% to the slope of the frequency dependent linewidth.

A likely culprit of g -strain in free-standing samples is the non-uniformity of defects. Dislocations, ionized impurities, and potential fluctuations are present in all samples, causing spatially varying crystal fields. The variations in the crystal field splitting, which have both axial and basal components, will depend on the distance from each source of strain. If Mg is randomly distributed throughout a sample, each Mg can be affected by a different crystal field that depends on the distance from nearby defects, including dislocations or an interface. In thick free-standing samples with a low dislocation density, Mg will be affected on average by a smaller Δ_x and therefore a greater variation in g_\perp will be observed [13]. The resulting EPR linewidth should be both anisotropic and frequency-dependent due to a large variation in g -factors within the sample, consistent with what is seen in free-standing crystals. If, however, the basal crystal field is large, as is predicted in thin-film samples due to a higher dislocation density and interfacial lattice mismatch, small deviations of the basal

crystal field should produce almost no variation in g -factors within the sample.

Conclusion

In this paper, we provide experimental evidence supporting the model for the Mg acceptor in GaN as that of a hole on a basal site. A crystal field analysis similar to that used to understand the g -factor anisotropy in thin films is shown to apply well to the angular dependence of the intensity. Further, the analysis is extended to a broad range of crystals, providing a more robust support to the basal site model. Additionally, the frequency-dependent linewidth observed in samples with a small basal crystal field confirms the predictions from previous authors of a linewidth dominated by g -strain that provides evidence that the crystal field around the Mg is non-uniform.

Acknowledgments

The authors would like to thank Sumner Harris and Dr Paul Baker for performing XRD measurements on GaN thin-films and free-standing samples. Also, we appreciate the assistance of Dr Alan Doolittle and Dr Andrew Allerman, who provided the thin-film samples used in this study and additionally Dr Marcin Zajac and Dr Michal Bockowski for providing amorphous samples. The work at UAB and FSU was supported by the National Science Foundation, Grant Numbers DMR-1606765 and DMR-1610226, respectively. The National High Magnetic Field Laboratory is supported by the National Science Foundation (cooperative agreements DMR-1157490 and DMR-1644779) and the State of Florida.

ORCID iDs

U R Sunay  <https://orcid.org/0000-0002-4074-9281>

References

- [1] Masui H, Nakamura S, DenBaars S P and Mishra U K 2010 Nonpolar and semipolar iii-nitride light-emitting diodes: achievements and challenges *IEEE Trans. Electron Devices* **57** 88
- [2] DenBaars S P *et al* 2013 Development of gallium–nitride-based light-emitting diodes (LEDs) and laser diodes for energy-efficient lighting and displays *Acta Mater.* **61** 945
- [3] Tompkins R P, Smith J R, Kirchner K W, Jones K A, Leach J H, Udway K, Preble E, Suvarna P, Leathersich J M and Shahedipour-Sandvik F 2014 GaN power Schottky diodes with drift layers grown on four substrates *J. Electron. Mater.* **43** 850
- [4] Jessen G H, Fitch R C, Gillespie J K, Via G, Crespo A, Langley D, Denninghoff D J, Trejo M and Heller E R 2007 Short-channel effect limitations on high-frequency operation of AlGaIn/GaN HEMTs for T-gate devices *IEEE Trans. Electron Devices* **54** 2589
- [5] Park H J, Park C, Yeo S, Kang S W, Mastro M, Kryliouk O and Anderson T J 2005 Epitaxial strain energy measurements of GaN on sapphire by Raman spectroscopy *Phys. Status Solidi c* **2** 446
- [6] Sugahara T, Sato H, Hao M, Naoi Y, Kurai S, Tottori S, Yamashita K, Nishino K, Romano L T and Sakai S 1998 Direct evidence that dislocations are non-radiative recombination centers in GaN *Japan. J. Appl. Phys.* **37** L398
- [7] Marino F A, Faralli N, Palacios T, Ferry D K, Goodnick S M and Saraniti M 2010 Effects of threading dislocations on AlGaIn/GaN high-electron mobility transistors *IEEE Trans. Electron Devices* **57** 353
- [8] Sugiura L 1997 Dislocation motion in GaN light-emitting devices and its effect on device lifetime *J. Appl. Phys.* **81** 1633
- [9] Sun Y Y, Abtew T A, Zhang P and Zhang S B 2014 Anisotropic polaron localization and spontaneous symmetry breaking: comparison of cation-site acceptors in GaN and ZnO *Phys. Rev. B* **90** 165301
- [10] Lyons J L, Janotti A and Van de Walle C G 2012 Shallow versus deep nature of Mg acceptors in nitride semiconductors *Phys. Rev. Lett.* **108** 156403
- [11] Kennedy T A, Glaser E R, Freitas J A, Carlos W E, Khan M A and Wickenden D K 1995 Native defects and dopants in GaN studied through photoluminescence and optically detected magnetic resonance *J. Electron. Mater.* **24** 219
- [12] Glaser E R, Murthy M, Freitas J A, Storm D F, Zhou L and Smith D J 2007 Optical and magnetic resonance studies of Mg-doped GaN homoepitaxial layers grown by molecular beam epitaxy *Physica B* **401–2** 327
- [13] Aliev G N, Zeng S, Davies J J, Wolverson D, Bingham S J, Parbrook P J and Wang T 2005 Nature of acceptor states in magnesium-doped gallium nitride *Phys. Rev. B* **71** 195204
- [14] Malyshev A V, Merkulov I A and Rodina A V 1998 Effective mass calculation of the shallow acceptor ground state *G*-factor for A3B5 semiconductors *Phys. Status Solidi* **210** 865
- [15] Alves H, Leiter F, Pfisterer D, Hofmann D M, Meyer B K, Einfeld S, Heinke H and Hommel D 2003 Mg in GaN: the structure of the acceptor and the electrical activity *Phys. Status Solidi* **1770**
- [16] Burnham S D, Namkoong G, Look D C, Clafin B and Doolittle W A 2008 Reproducible increased Mg incorporation and large hole concentration in GaN using metal modulated epitaxy *J. Appl. Phys.* **104** 024902
- [17] Zvanut M E, Dashdorj J, Freitas J A, Glaser E R, Willoughby W R, Leach J H and Udway K 2016 Incorporation of Mg in free-standing HVPE GaN substrates *J. Electron. Mater.* **45** 2692
- [18] Tompkins R P *et al* 2013 HVPE GaN for high power electronic schottky diodes *Solid-State Electron.* **79** 238
- [19] Zvanut M E, Dashdorj J, Sunay U R, Leach J H and Udway K 2016 Effect of local fields on the Mg acceptor in GaN films and GaN substrates *J. Appl. Phys.* **120** 135702
- [20] Mola M, Hill S, Goy P and Gross M 2000 Instrumentation for millimeter-wave magnetoelectrodynamic investigations of low-dimensional conductors and superconductors *Rev. Sci. Instrum.* **71** 186
- [21] Patel J L, Nicholls J E and Davies J J 1981 Optically detected magnetic resonance of two shallow acceptor centres in cadmium sulphide *J. Phys. C: Solid State Phys.* **14** 1339
- [22] Wertz J E and Bolton J R 1986 *Electron Spin Resonance* 1st edn (Berlin: Springer)
- [23] Stępniewski R, Wyszomolek A, Potemski M, Pakula K, Baranowski J M, Grzegory I, Porowski S, Martinez G and Wyder P 2003 Fine structure of effective mass acceptors in gallium nitride *Phys. Rev. Lett.* **91** 226404
- [24] Misra P, Behn U, Brandt O, Grahn H T, Imer B, Nakamura S, DenBaars S P and Speck J S 2006 Polarization anisotropy in GaN films for different nonpolar orientations studied by polarized photoreflectance spectroscopy *Appl. Phys. Lett.* **88** 161920
- [25] Ham F S 1965 Dynamical Jahn–Teller effect in paramagnetic resonance spectra: orbital reduction factors and partial quenching of spin-orbit interaction *Phys. Rev.* **138** A1727
- [26] Aasa R and Vänngård T 1975 EPR signal intensity and powder shapes: a reexamination *J. Magn. Reson.* **19** 308
- [27] Pilbrow J 1984 Lineshapes in frequency-swept and field-swept EPR for spin 1/2* *J. Magn. Reson.* **58** 186
- [28] Glaser E R, Kennedy T A, Doverspike K, Rowland L B, Gaskill D K, Freitas J A, Asif Khan M, Olson D T, Kuznia J N and Wickenden D K 1995 Optically detected magnetic resonance of GaN films grown by organometallic chemical-vapor deposition *Phys. Rev. B* **51** 13326
- [29] Davydov V Y, Averkiev N S, Goncharuk I N, Nelson D K, Nikitina I P, Polkovnikov A S, Smirnov A N, Jacobson M A and Semchinova O K 1997 Raman and photoluminescence studies of biaxial strain in GaN epitaxial layers grown on 6H–SiC *J. Appl. Phys.* **82** 5097
- [30] Stoneham A M 1966 The theory of the strain broadened line shapes of spin resonance and optical zero phonon lines *Proc. Phys. Soc.* **89** 909